

# Magnetic Force Microscope Contrast Simulation for Low-Coercive Ferromagnetic and Superparamagnetic Nanoparticles in an External Magnetic Field

Victor L. Mironov<sup>1</sup>, Dmitry S. Nikitushkin<sup>1</sup>, Chris Bins<sup>2</sup>, Andrey B. Shubin<sup>3</sup>, and Peter A. Zhdan<sup>4</sup>

<sup>1</sup>Institute for physics of microstructures RAS, 603950 Nizhny Novgorod, Russia

<sup>2</sup>Department of Physics and Astronomy, University of Leicester, Leicester LE1 7RH, U.K.

<sup>3</sup>“Nanotechnology MDT” Company, 124482 Zelenograd, Russia

<sup>4</sup>School of Engineering, University of Surrey, Guildford, Surrey GU2 7XH, U.K.

We report the results of simulations of magnetic force microscope (MFM) contrast for low-coercive ferromagnetic and superparamagnetic nanoparticles. We show that two types of MFM contrast in the form of gaussian and ring distributions can be observed because of probe-particle interaction. We discuss stabilization of the magnetic moment of nanoparticles by an external magnetic field. We have calculated the values of stabilizing magnetic fields and their dependence on probe parameters and scanning heights.

**Index Terms**—Low-coercive magnetic nanoparticles, magnetic force microscopy, superparamagnetic particles.

## I. INTRODUCTION

SIZE reduction of the magnetic memory elements is a fundamental requirement in the development of modern magnetic data storage systems [1]–[3]. As a result, investigations of the magnetic states in small magnetic particles by magnetic force microscopy methods (MFM) have a great importance. One of the substantial problems is registration and interpretation of MFM images from such objects [4]–[7]. In this case, MFM contrast is formed in conditions of strong interaction between the probe field and the particle magnetic moment, which leads to difficulties in the interpretation of experimental results. Here, we report the results of model calculations and computer simulations of MFM contrast for low-coercive (LC) ferromagnetic and superparamagnetic (SP) nanoparticles in external magnetic fields, which explain some peculiarities in the experimental MFM images.

## II. MFM CONTRAST SIMULATION FOR LOW COERCIVE FERROMAGNETIC PARTICLES

In the calculations, the MFM tip was approximated as a uniform magnetized sphere (Fig. 1) with an effective magnetic moment  $m_t = M_t V_t$  ( $M_t$  is the remanent magnetization of the tip capping material and  $V_t$  is the effective volume of the interactive part of the tip). The probe field was represented as the field of a single magnetic dipole [8], [9].

Analysis of experimental data shows that the typical effective volume of magnetic material for our probes with Co coating ( $M_t \sim 1400$  G) is approximately  $10^5$  nm<sup>3</sup>. We also assume that particles have uniform magnetization and the direction of their moment is completely defined by the external magnetic field. The distribution of phase shift  $\Delta\varphi$  for cantilever oscillations was calculated as model MFM images:

$$\Delta\varphi = \frac{Q}{K} \frac{\partial F_z}{\partial z} \quad (1)$$

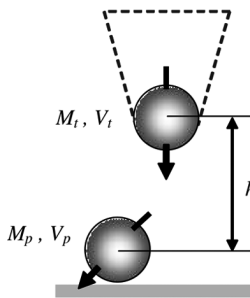


Fig. 1. Schematic picture of the MFM probe and LC particle.

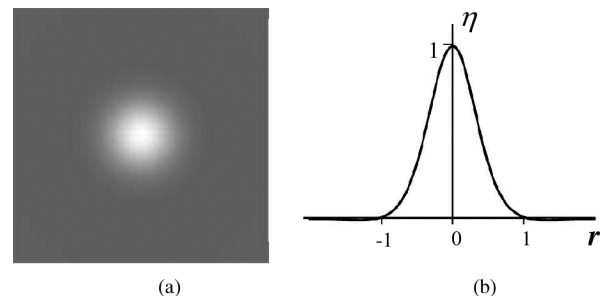


Fig. 2. MFM contrast (a) and its central cross section (b) for spherical LC particle. Here,  $\eta = (\Delta\varphi)/(\Delta\varphi_{LC}^*)$ ,  $r = (x/h) \cdot \Delta\varphi_{LC}^*$  is the phase contrast in maximum.

where  $Q$  is the cantilever quality factor,  $K$  is the cantilever force constant, and  $F_z$  is the force Z-component. Spherical and cylindrical single-domain Co particles with characteristic diameters in the range of 50 to 20 nm and a coercive field  $H_c$  lower than the field of MFM probe:  $H_c \ll H_t$  were considered as LC particles. The calculations were performed in the dipole-dipole approximation. Particles were represented as the point dipoles with magnetic moment  $m_p = M_p V_p$  ( $M_p$  is the saturation magnetization and  $V_p$  is the particle volume). Results of computer simulation for MFM contrast from spherical nanoparticle are represented in Fig. 2(a) and (b).

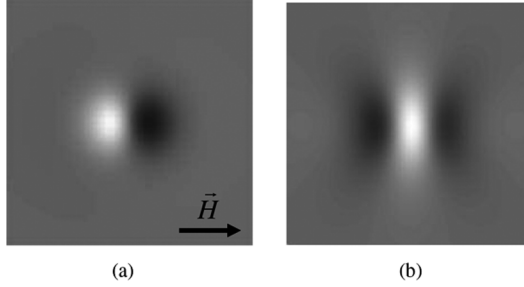


Fig. 3. MFM contrast for spherical Co particle with 50 nm diameter in the strong external field. (a)  $H_{\text{ex}} \gg H_t$ . (b)  $H_{\text{ex}} \gg H_{\text{ct}}$ . Scanning height is 50 nm.

MFM contrast in maximum is defined by the following expression:

$$\Delta\varphi_{\text{LC}}^*(h) = \frac{2\pi^2 Q M_p d_p^3 M_t d_t^3}{3K h^5} \quad (2)$$

where  $d_p$  is the particle diameter,  $d_t$  is the effective diameter of the MFM probe, and  $h$  is the separation between the spherical probe and particle centers (scanning height). The section curve [Fig. 2(b)] crosses the abscissa axis in the  $r = \pm 1.055 \cdot h$  points. As is clearly seen in Fig. 2(a), phase MFM contrast from small spherical particles has the same symmetry as amplitude tapping mode contrast caused by the Van-der-Waals interaction that essentially complicates analysis and interpretation of MFM measurements [5], [6]. In this situation, an external uniform magnetic field  $H_{\text{ex}}$  applied in the sample plane can help to separate the contribution of the magnetic interaction in the MFM phase contrast. The calculations show that the MFM image (Fig. 2) is transformed under increasing  $H_{\text{ex}}$  so in a strong magnetic field  $H_{\text{ex}} > H_t$  MFM contrast distribution has bright and black poles, which correspond to the image from the particle uniformly magnetized along  $\vec{H}_{\text{ex}}$  [Fig. 3(a)]. At last when  $H_{\text{ex}} > H_{\text{ct}}$  (where  $H_{\text{ct}}$  is the coercive field for the probe) the magnetic moment of the probe is directed along  $\vec{H}_{\text{ex}}$  and MFM contrast distribution has two black and one bright pole [Fig. 3(b)].

The MFM contrast transformation under increasing  $H_{\text{ex}}$  is represented in Fig. 4(a). In extremely high magnetic fields, the distance between minimum and maximum in MFM contrast is equal to  $\Delta x_\infty = h/\sqrt{2}$ . It should be noted that magnetic contrast distribution transforms in the external field practically without a decrease of contrast amplitude [Fig. 4(b)]. The value of magnetic field, which stabilizes contrast on the level 90% from  $\Delta\varphi_\infty$  (contrast minimum in extremely high magnetic field) equals  $H_{0.9} = 11 \cdot (M_t V_t)/(h^3)$  and is defined by tip parameters and scanning height.

A similar situation is observed for the particles in the form of circular discs. It was assumed that the magnetic moment is freely rotated in the disc plane. The MFM image for the circular disc without external field has a ring distribution of the phase contrast [Fig. 5(a)]. If a uniform magnetic field is applied in the sample plane, MFM contrast redistribution is observed [Fig. 5(b) and (c)].

It is clearly seen that MFM contrast in the strong magnetic field corresponds to the MFM image from the particle with uniform magnetization [Fig. 5(c)].

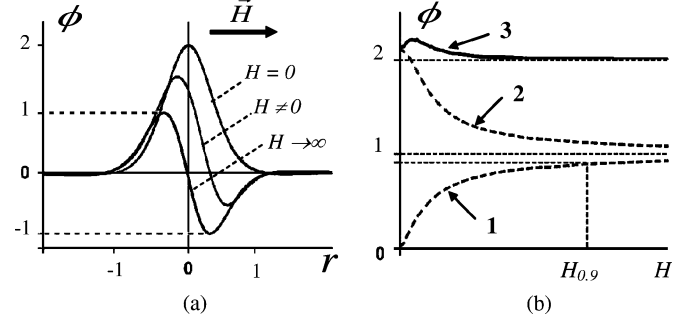


Fig. 4. (a) is changing of MFM contrast cross section for spherical LC particle under increasing of  $H_{\text{ex}}$  from 0 to  $\infty$ . Here  $\phi = (\Delta\varphi)/(\Delta\varphi_\infty)$ ,  $r = (x/h)$  (where  $\Delta\varphi_\infty$  is value of minimum contrast at  $H_{\text{ex}} = \infty$ ); (b) is MFM contrast dependence for LC particle on external magnetic field: 1 is dependence for module of MFM contrast minimum, 2 is dependence for value of contrast maximum, and 3 is difference between maximum and minimum of MFM contrast.

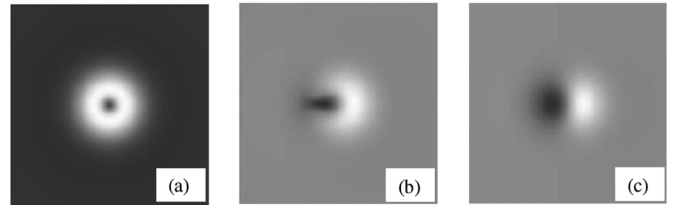


Fig. 5. Simulated MFM contrast from the Co circular disc with 50 nm diameter and 20 nm height in the external magnetic field. (a)  $H = 0$ ; (b)  $H = 0.5$  kOe; (c)  $H = 5$  kOe. Scanning height is 50 nm.

### III. MFM CONTRAST SIMULATION FOR SUPERPARAMAGNETIC PARTICLES

The peculiarities of MFM contrast formation from SP particles were considered for spherical Co particles with characteristic sizes less than 10 nm. The magnetic moment of such particles experiences thermal fluctuations and can be approximated by the Langevin function  $L(\alpha)$  [10], [11]

$$m = m_0 L\left(\frac{m_0 H}{kT}\right) = m_0 \left( \coth \frac{m_0 H}{kT} - \frac{kT}{m_0 H} \right) \quad (3)$$

where  $k$  is Boltzmann constant,  $T$  is temperature,  $H$  is the external magnetic field, and  $m_0 = M_p V_p$  is the particle magnetic moment in saturation.

The symmetry of MFM contrast for LC and SP particles are practically the same (Fig. 6). The difference is only in the amplitude of the phase contrast for the SP particle, which is defined by the following expression:

$$\Delta\varphi_{\text{SP}}^*(h) = \frac{2\pi^2 Q M_p d_p^3 M_t d_t^3}{3K h^5} \left( \coth \alpha(h) - \frac{1}{\alpha(h)} \right) \quad (4)$$

$$\alpha(h) = \frac{\pi^2 M_p M_t d_p^3 d_t^3}{18kT h^3} \quad (5)$$

which is distinguished from  $\Delta\varphi_{\text{LC}}^*$  by Langevin function  $L(\alpha)$ .

The value of the magnetic moment reaches 0.9  $M_s$  for a value of the argument  $\alpha^* \sim 10$  (see Fig. 7). It allows us to estimate value of the magnetic field that stabilizes the magnetic moment of the SP particle

$$H^* = \alpha^* \frac{kT}{M_p V_p}. \quad (6)$$

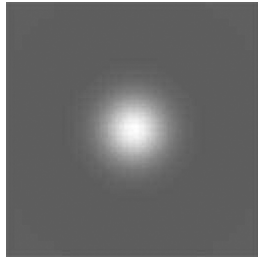


Fig. 6. MFM contrast distribution for spherical SP particle.

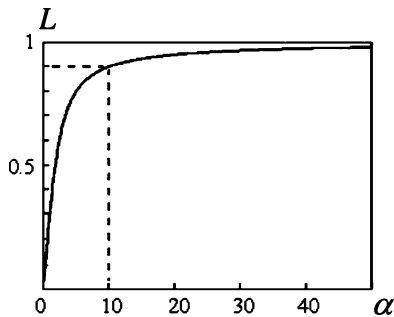
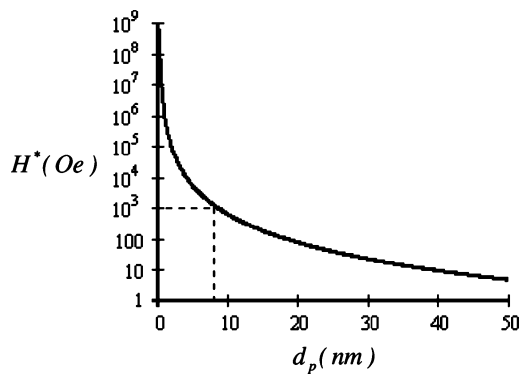


Fig. 7. Langevin function.

Fig. 8. Dependence of  $H^*$  on particle diameter  $d_p$  at room temperature.

It is possible on the basis of criterion (6) to estimate the scanning height parameter that will realize the effective MFM contrast formation for the SP particle. The condition  $H_t > H^*$  leads us to the following inequalities:

$$\frac{d_p + d_t}{2} < h < d_p d_t \sqrt[3]{\frac{\pi^2 M_p M_t}{\alpha^* 18 k T}}. \quad (7)$$

The parameter  $H^*$  depends on the particle volume and temperature (6). The dependence of  $H^*$  value on particle diameter  $d_p$  at room temperature is represented in Fig. 8.

As is shown in Fig. 8, stabilization of the magnetic moment for a field 1 kOe (characteristic value of magnetic fields for *in situ* MFM measurements) is possible only for SP particles with diameters greater than 8 nm. To stabilize particles with  $d_p < 8$  nm, high magnetic fields should be used or measurements performed at low temperature.

#### IV. CONCLUSION

The analytical calculations and computer simulations of the MFM contrast from small low coercive ferromagnetic and superparamagnetic particles in an external magnetic field were performed. It was shown that two types of MFM contrast in the form of gauss and ring distributions caused by probe-particle interaction can be formed. The external magnetic field applied in the sample plane stabilizes the magnetic moment of nanoparticles. It leads to the MFM contrast transformation which allows separation of contributions from Van-der-Waals and magnetic interactions in the MFM phase images. The possibility of MFM contrast observation from superparamagnetic Co particles in strong magnetic fields was demonstrated. The values of stabilizing magnetic fields and their dependence on probe parameters and scanning heights for low-coercive ferromagnetic and superparamagnetic nanoparticles were calculated.

#### ACKNOWLEDGMENT

This work was supported in part by RFBR (Project 05-02-17153) and by EC through the NANOSPIN project (Contract NMP4-CT-2004-013545). The authors are thankful to Prof. A.A. Fraerman (Institute for physics of microstructures RAS) for the very useful discussions.

#### REFERENCES

- [1] J. I. Martin, J. Nogues, K. Liu, J. L. Vincent, and I. K. Schuller, "Ordered magnetic nanostructures: Fabrication and properties," *J. Magn. Magn. Mater.*, vol. 256, pp. 449–501, 2003.
- [2] A. Kikitsu, Y. Kamata, M. Sakurai, and K. Naito, "Recent progress of patterned media," *IEEE Trans. Magn.*, vol. 43, no. 9, pp. 3685–3688, Sep. 2007.
- [3] H. J. Richter, A. Y. Dobin, O. Heinonen, K. Z. Gao, R. J. M. v. d. Veerdom, R. T. Lynch, J. Xue, D. Weller, P. Asselin, M. F. Erden, and R. M. Brockie, "Recording on bit-patterned media at densities of 1 Tb/in<sup>2</sup> and beyond," *IEEE Trans. Magn.*, vol. 42, no. 10, pp. 2255–2260, Oct. 2006.
- [4] M. Rasa and A. P. Philipse, "Scanning probe microscopy on magnetic colloidal particles," *J. Magn. Magn. Mater.*, vol. 252, pp. 101–103, 2002.
- [5] M. Rasa, B. W. M. Kuipers, and A. P. Philipse, "Atomic force microscopy and magnetic force microscopy study of model colloids," *J. Colloid Interface Sci.*, vol. 250, pp. 303–315, 2002.
- [6] S. A. Koch, R. H. te Velde, G. Palasantzas, and J. Th. M. De Hosson, "Magnetic versus structural properties of Co nanocluster thin films: A magnetic force microscopy study," *Appl. Phys. Lett.*, vol. 84, no. 4, pp. 556–558, Jan. 2004.
- [7] S. A. Koch, R. H. te Velde, G. Palasantzas, and J. Th. M. De Hosson, "Magnetic force microscopy on cobalt nanocluster films," *Appl. Surf. Sci.*, vol. 226, pp. 185–190, 2004.
- [8] U. Hartmann, "The point dipole approximation in magnetic force microscopy," *Phys. Lett. A*, vol. 137, pp. 475–479, 1989.
- [9] Th. Kebe and A. Carl, "Calibration of magnetic force microscopy tips by using nanoscale current-carrying parallel wires," *J. Appl. Phys.*, vol. 95, no. 3, pp. 775–792, Feb. 2004.
- [10] C. Kittel, *Introduction to Solid State Physics*, 7th ed. New York: Wiley, 1996.
- [11] D. C. Douglass, A. J. Cox, J. P. Bucher, and L. A. Bloomfield, "Magnetic properties of free cobalt and gadolinium clusters," *Phys. Rev. B*, vol. 47, no. 19, pp. 12874–12889, May 1993.